Materials Research Proceedings 31 (2023) 596-613 https://doi.org/10.21741/9781644902592-62

Linear response of thin axysimmetric cross-ply structure under a static load: Numerical and analythical comparisons

Salvatore Saputo [1 *], Erasmo Carrera [1], Volodymyr V. Zozulya [2]

[1]Department of Aeronautics and Aerospace Engineering, Politecnico di Torino, Corso Duca degli Abruzzi, 24, 10129 Torino, Italy

[2]S. P. Timoshenko Institute of Mechanics, National Academy of Sciences of Ukraine, Nesterov Str. 3, 252680 Kyiv, Ukraine

*salvatore.saputo@polito.it

Keywords: Carrera Unified Formulation, Higher-Order Theories, Analytical Solution, Bending, Laminated Composite Plate

Abstract. Thin-walled mechanical components, such as beams, plates and shells, are widely used as structural components in several engineering fields, in particular mechanical, aeronautical and aerospace sectors. The purpose of this work is to analyse the cross-ply bending behaviour of cylindrical and spherical shell structures using the finite element method. Hence, numerical models, realized using commercial software, were realized using the shell and solid approaches and were compared with numerical and analytical methods to appreciate their advantages. In this research, a Navier solution in close form for high-order theories, developed using the Carrera Unified Formulation (CUF) approach, has been reported, where the high-order elastic shell model has been developed using the variational principle of virtual work for three-dimensional linear theory equations and the analytical results were obtained using the Mathematica software. The results furnished by the numerical method such as the elasticity solutions given in the literature using Navier's method are used as a benchmark for comparing the finite element method results in terms of maximum displacement and stress distribution along the principal structure direction. However, the numerical shell model cannot provide sufficient data to describe the tensional and deformational state at all points and especially along the laminate thickness. Wishing to obtain a complete description of the plate's mechanical behaviour, it is necessary to use a three-dimensional approach with the associated increase in calculation time. In contrast, the numerical solution based on the CUF approach shows a very efficient description of the composite structure behaviour and its use should be preferred to the classical lamination approach if an accurate description of the structure is necessary.

Introduction

Layered structures are being employed more and more in automotive, aerospace and naval vehicles. Throughout the latter half of the 20th century, composite materials were developed and adopted in areas where a high stiffness-to-weight ratio was required. There are modern examples of aircraft for military and civil uses as well as boats, helicopters, ultralights and gliders, whose structure is made exclusively of composite material. Layered structures choice, noticeably, complicates the design, analysis, and manufacturing processes. All these aspects adding to the difficulties already known regarding the use of conventional isotropic materials. Moreover, the high discontinuity in the mechanical properties of layered structures, due to their nature, requires the ZZ (zig zag) theory for the description of stress and displacement along thickness as well as interlaminar continuity (in-plane and out-of-plane stresses) [1][2] that greatly complicate the analysis of such structures. Analytical closed-form solutions are only available for extremely simple geometries. The resolution of more complex layered structures geometry and/or boundary conditions is left to numerical methods with different approximation values. Many authors

Materials Research Proceedings 31 (2023) 596-613 https://doi.org/10.21741/9781644902592-62

proposed different numerical technique in order to evaluate the deformation and the stress distribution in every point of the structure. Noor and Raig [3] proposed a 3D finite difference technique for axial symmetric multilayer structure. Malik and Liew [4][5] proposed a differential quadrature technique for complex structure. A meshless collocation method, set on radial basis function, have been adopted by Ferreira et al [6][7] to analyse laminated plates and shells. For a comprehensive overview of different computational methods and their uses related to layered structure can be found in [8][9][10]. A particular focus should be posed on the finite element method (FEM) that is widely adopted to study the mechanical behaviour of the composite structure. Moreover, different finite element methods are based on axiomatic-type theories where the unknown variables are suggested along the thickness. In particular, the earliest FEM calculation are based on the classical Kirchhoff-Love theory [11][12][13][14][15]. However, it was challenging to meet the compatibility requirements in thin shell analysis because rotations were derived from transversal displacement, and to avoid this issue, plate/shell elements based on the first-order shear deformation theory (FSDT) were developed by several authors [16][17][18]. Severe stiffening limits for thin plate are showed by newest FSDT finite elements, known as shear locking. However, early FSDT-type elements showed severe stiffening in thin plate/shell limits, which resulted in a numerical mechanism known as shear or membrane locking. This locking was initially countered by implementing numerical tricks, operating on the integration schemes [19], but they introduced spurious zero energy modes. A solution to this problem is proposed by Naghdi [20], where the shell finite element could counteract the locking problem in its displacement formulation. On the other hand, if the element is not of high enough degree and the thickness is very small, the numerical solution may exhibit a loss in the rate of convergence due to locking. To avoid both the mentioned problem the mixed interpolation of tensorial component approach (MITC) can be adopted as treated by several authors [21][22][23][24]. In the past two decades, numerous plate and shell finite element approaches have been suggested, using higher-order theories (HOT). Kant et al. [25] introduced HOT- finite elements that necessitate continuity only for the unknown variables and not for their derivatives. Otherwise, Polit et al [26]. developed a C^1 six-node triangular finite element using cosine functions to represent transverse shear strains. With this approach the continuity of displacement and shear stress was ensure between the interface of the layered structure. Tessler [27] has provided a comprehensive analysis of HOT-type theories and their suitability for finite element applications. Several other studies have implemented HOTs for plates and shells, and additional information can be found in the literature [28]. There have been many proposals for finite elements based on zigzag theories, such as Rao and Meyer-Piening that suggested using the Reissner mixed variational theorem (RMVT) to develop standard finite elements.[29]. Lastly, several authors, including Noor and Burton [30], Reddy [31], and Rammerstorfer et al. [32] have proposed finite element implementations of layer-wise theories in the framework of axiomatic-type theories.

A new and improved shell finite element is introduced for the analysis of composite structures [33][34], based on Carrera's Unified Formulation (CUF), which was originally developed by Carrera for multi-layered structures [35][36]. The new shell finite element includes both equivalent single layer (ESL) and layer-wise (LW) theories found in CUF. In this work, several shell-based finite element theories were introduced and compared to analyse the mechanical response of layered structures with different geometry. Comparisons are made between classical theories such as CST and FSDT, analytical type solutions, commercial code and CUF high order approaches. Three different geometries were used, such as a plate, a cylindrical section and a cylinder. Finally, different thicknesses were evaluated for each geometry to highlight the limits of the various theories.

Materials Research Proceedings 31 (2023) 596-613 https://doi.org/10.21741/9781644902592-62

Unified form building up of plate theories in terms of a few "fundamental nuclei" with variational statements.

Considering theories that assume displacement and transverse shear and normal stress in the axiomatic approach, the displacement or stress fields are postulated in the plate's z-direction. Typically, two-dimensional theories are build up following four steps: assigning material behavior (e.g. Hooke's Law); suppose a geometrical relation (e.g. strain-displacement relation); postulating displacement and/or stress distributions in the thickness of the plate's z-direction by stating to a set of base functions; and finally, utilizing an appropriate variational statement (PVD or RMVT) to determine governing equations and boundary conditions which are variationally consistent with the hypotheses introduced in the first three steps. The aim of this discussion is to explore theories within the scope of the PVD and the RMVT.

Hooke's law:

The multilayered plates composed of N_l layers, shown in Figure 1, have a geometry and Cartesian coordinate system *x, y, z*. The laminae are assumed to be homogenous and to be functioning within the linear elastic range. Standard form for Hooke's law is applied for the anisotropic k-lamina stiffness coefficients.

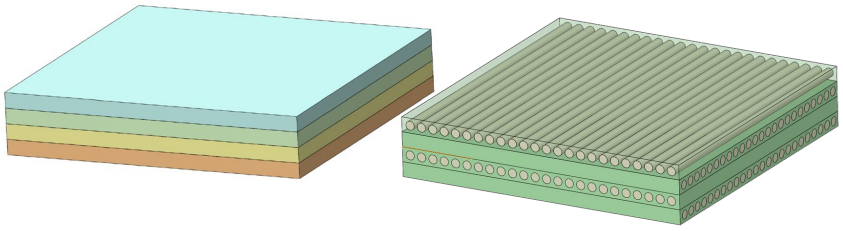

Figure 1 Multi-layered structure

The Hooke's Law reads $\sigma_i = \tilde{C}_{ij}\epsilon_j$ where sub-indices *i* and *j*, ranging from 1 to 6, stand for the index couples 11, 22, 33, 13, 23 and 12, respectively. The material is supposed to be orthotropic as specified by $\tilde{C}_{14} = \tilde{C}_{24} = \tilde{C}_{34} = \tilde{C}_{64} = \tilde{C}_{15} = \tilde{C}_{25} = \tilde{C}_{35} = \tilde{C}_{65} = 0$. This implies that ${\sigma^k}_{xz}$ and ${\sigma^k}_{yz}$ depend only on ${\epsilon^k}_{xz}$ and ${\epsilon^k}_{yz}$. In matrix form:

$$\begin{aligned} {\boldsymbol{\sigma}^k}_{p\mathrm{H}} &= \tilde{\boldsymbol{C}}^k_{pp}\boldsymbol{\epsilon}^k_{p\mathrm{G}} + \tilde{\boldsymbol{C}}^k_{pn}\boldsymbol{\epsilon}^k_{n\mathrm{G}} \\ {\boldsymbol{\sigma}^k}_{n\mathrm{H}} &= \tilde{\boldsymbol{C}}^k_{np}\boldsymbol{\epsilon}^k_{p\mathrm{G}} + \tilde{\boldsymbol{C}}^k_{nn}\boldsymbol{\epsilon}^k_{n\mathrm{G}} \end{aligned} \tag{1}$$

where,

$$\tilde{\boldsymbol{C}}^k_{pp} = \begin{bmatrix} \tilde{C}^k_{11} & \tilde{C}^k_{12} & \tilde{C}^k_{16} \\ \tilde{C}^k_{12} & \tilde{C}^k_{22} & \tilde{C}^k_{26} \\ \tilde{C}^k_{16} & \tilde{C}^k_{26} & \tilde{C}^k_{66} \end{bmatrix}, \tilde{\boldsymbol{C}}^k_{pn} = \tilde{\boldsymbol{C}}^{k\mathrm{T}}_{np} = \begin{bmatrix} 0 & 0 & \tilde{C}^k_{13} \\ 0 & 0 & \tilde{C}^k_{23} \\ 0 & 0 & \tilde{C}^k_{36} \end{bmatrix}, \tilde{\boldsymbol{C}}^k_{nn} = \begin{bmatrix} \tilde{C}^k_{44} & \tilde{C}^k_{45} & 0 \\ \tilde{C}^k_{45} & \tilde{C}^k_{55} & 0 \\ 0 & 0 & \tilde{C}^k_{66} \end{bmatrix}$$

Bold letters represent arrays. The superscript 'T' indicates array transposition. The subscripts *n* and *p* denote transverse (out-of-plane, normal) and in-plane values, respectively. Therefore

$$\boldsymbol{\sigma}^k_p = \{\sigma^k_{xx}, \sigma^k_{yy}, \sigma^k_{xy}\}, \qquad \boldsymbol{\sigma}^k_n = \{\sigma^k_{xz}, \sigma^k_{yz}, \sigma^k_{zz}\}$$

$$\boldsymbol{\epsilon}^k_p = \{\epsilon^k_{xx}, \epsilon^k_{yy}, \epsilon^k_{xy}\}, \qquad \boldsymbol{\epsilon}^k_n = \{\epsilon^k_{xz}, \epsilon^k_{yz}, \epsilon^k_{zz}\}.$$

Subscript 'H' denotes stresses assessed by Hooke's law whereas subscript 'G' denotes strain from the geometrical relation Eq. (3).

Eq. (1) is employed together with a regular displacement formulation based on the principles of PVD, and the stress-strain relationships are expressed in a blended form for the integrated solution procedure:

$$\begin{aligned} \boldsymbol{\sigma}_{p\mathrm{H}}^{k} &= \boldsymbol{C}_{pp}^{k}\boldsymbol{\epsilon}_{p\mathrm{G}}^{k} + \boldsymbol{C}_{pn}^{k}\boldsymbol{\sigma}_{nM}^{k} \\ \boldsymbol{\epsilon}_{n\mathrm{H}}^{k} &= \boldsymbol{C}_{np}^{k}\boldsymbol{\epsilon}_{p\mathrm{G}}^{k} + \boldsymbol{C}_{nn}^{k}\boldsymbol{\sigma}_{nM}^{k} \end{aligned} \tag{2}$$

using both stiffness and compliance coefficients. To link the two expressions of Hooke's law, the following can be deduced:

$$\begin{aligned} \boldsymbol{C}_{pp}^{k} &= \widetilde{\boldsymbol{C}}_{pp}^{k} - \widetilde{\boldsymbol{C}}_{pn}^{k}\widetilde{\boldsymbol{C}}_{nn}^{k^{-1}}\widetilde{\boldsymbol{C}}_{np}^{k}, \qquad \boldsymbol{C}_{pn}^{k} = \widetilde{\boldsymbol{C}}_{pn}^{k}\widetilde{\boldsymbol{C}}_{nn}^{k^{-1}} \\ \boldsymbol{C}_{np}^{k} &= -\widetilde{\boldsymbol{C}}_{nn}^{k^{-1}}\widetilde{\boldsymbol{C}}_{np}^{k}, \qquad \boldsymbol{C}_{nn}^{k} = \widetilde{\boldsymbol{C}}_{nn}^{k^{-1}} \end{aligned}$$

Superscript '-1' denotes an inversion of the array.

Geometrical relation:

The strain components $\boldsymbol{\epsilon}_{p}^{k}, \boldsymbol{\epsilon}_{n}^{k}$ are linearly related to the displacements $\boldsymbol{u}^{k}\left(\left\{u_{x}^{k}, u_{y}^{k}, u_{z}^{k}\right\}\right)$ according to the following geometrical (subscript G) relations:

$$\boldsymbol{\epsilon}_{p\mathrm{G}}^{k} = D_{p}\boldsymbol{u}^{k}, \qquad \boldsymbol{\epsilon}_{n\mathrm{G}}^{k} = D_{n}\boldsymbol{u}^{k} \tag{3}$$

D_p and D_n denotes in-plane and out-of-plane differential operators:

$$D_{p} = \begin{bmatrix} \partial_{x} & 0 & 0 \\ 0 & \partial_{y} & 0 \\ \partial_{y} & \partial_{x} & 0 \end{bmatrix}; \qquad D_{n} = \begin{bmatrix} \partial_{z} & 0 & \partial_{x} \\ 0 & \partial_{z} & \partial_{y} \\ 0 & 0 & \partial_{z} \end{bmatrix}.$$

Displacement and transverse assumptions:

The performance of a displacement and/or strain parameter f are assumed to be in accordance with a given expansion in the z-direction of the plate.

$$f(x,y,z) = F_{i}(z)\, f_{i}(x,y) \quad i = 0,1,\ldots,N. \tag{4}$$

The sum of the iterative indices i is computed over its domain. The polynomials $F_i(z)$ generate a group of individual functions and, this selection can be made arbitrarily. The magnitude of the projected expansion is expressed by N.

The use of displacement and transverse normal stress assumptions will result in this equation:

$$\begin{aligned} \boldsymbol{u}(x,y,z) &= F_{i}(z)\boldsymbol{u}_{i}(x,y) \\ \boldsymbol{\sigma}_{nM}(x,y,z) &= F_{i}(z)\boldsymbol{\sigma}_{n_{i}}(x,y) \end{aligned} \qquad i = 0,1,N. \tag{5}$$

M (as in model) has been introduced to separate the stresses assumed from those obtained from Hooke's law. In the numerical analysis, $N \leq 4$ will be accounted for. N can be unique for each variable as discussed in [37]. The conditions in Eq. (5) can be applied to either a single layer (LW) or multiple layers (ES).

Materials Research Proceedings 31 (2023) 596-613 https://doi.org/10.21741/9781644902592-62

Governing equations via PVD and RMVT:
For a multilayered plate subjected to static loadings,
PVD states

$$\sum_{k=1}^{N_l} \int_{\Omega^k}^{\Gamma^k} \int_{A_k}^{V} \left(\delta \boldsymbol{\epsilon}_{p_G}^{k\mathrm{T}} \boldsymbol{\sigma}_{pHd}^{k} + \delta \boldsymbol{\epsilon}_{n_G}^{k\mathrm{T}} \boldsymbol{\sigma}_{nH_d}^{k} \right) \, \mathrm{d}\Omega^k \mathrm{d}z \; = \delta L_e \tag{6}$$

δ is the variational symbol. A_k and V denote the layer thickness domain and volume; Ω^k is the layer middle surface bounded by Γ^k. The variation of the internal work has been split into in-plane and out-of-plane parts and involves stress from Hooke's Law and strain from geometrical relations. δL_e is the virtual variation of the work made by the external layer-forces $\boldsymbol{p}^k = \{p_x^k,\ p_y^k,\ p_z^k\}$. By replacing the variables in Eq.(1), Eq.(3), and the first Eq.(5) with suitable terms, a variational statement can be formulated that yields a set of equilibrium equations and boundary conditions. These equilibrium equations can be expressed concisely in the form:

$$\delta \boldsymbol{u}_\tau^k \,:\, \boldsymbol{K}_d^{k\tau s} \, \boldsymbol{u}_s^k \;=\; \boldsymbol{p}_\tau^k \tag{7}$$

The related boundary conditions are:

$$\boldsymbol{u}_\tau^k \;=\; \overline{\boldsymbol{u}}_\tau^k \; or \; \boldsymbol{\Pi}_d^{k\tau s} \boldsymbol{u}_s^k \;= \boldsymbol{\Pi}_d^{k\tau s} \overline{\boldsymbol{u}}_s^k \tag{8}$$

The number of equations derived is equal to the number of variables introduced: τ and s vary from 0 to N and k range from 1 to N_l. $\boldsymbol{K}$ and $\boldsymbol{\Pi}$ are arrays constitute by differential operators.
Reissner's mixed theorem [38][39] expresses both equilibrium and compatibility in relation to the unknowns $\boldsymbol{u}^k$ and $\boldsymbol{\sigma}_n^k$. This is achieved by means of the variational equation given below:

$$\sum_{k=1}^{N_l} \int_{\Omega^k}^{\Gamma^k} \int_{A_k}^{V} \left(\delta \boldsymbol{\epsilon}_{p_G}^{k\mathrm{T}} \boldsymbol{\sigma}_{p_H}^{k} + \delta \boldsymbol{\epsilon}_{n_G}^{k\mathrm{T}} \boldsymbol{\sigma}_{n_M}^{k} \;+\; \delta \boldsymbol{\sigma}_{n_M}^{k\mathrm{T}} \left(\boldsymbol{\epsilon}_{n_G}^{k} - \; \boldsymbol{\epsilon}_{n_H}^{k} \right) \right) \mathrm{d}\Omega^k \mathrm{d}z = \delta L^e \tag{9}$$

The LHS incorporates the changes of the internal force within the plate, with the initial two terms deriving from the displacement formulation, which lead to a balance of forces. The third term is a combined term which ensures the compatibility of the transverse strain components. The whole equation, expressed in terms of displacement and stress, is summarized in a concise form as follows:

$$\begin{aligned} &\delta \boldsymbol{u}_\tau^k \;:\; \boldsymbol{K}_{uu}^{k\tau s} \boldsymbol{u}_s^k + \boldsymbol{K}_{u\sigma}^{k\tau s} \boldsymbol{\sigma}_{ns}^k = \boldsymbol{p}_\tau^k \\ &\delta \boldsymbol{u}_{n\tau}^k \;:\; \boldsymbol{K}_{\sigma u}^{k\tau s} \boldsymbol{u}_s^k + \boldsymbol{K}_{\sigma\sigma}^{k\tau s} \boldsymbol{\sigma}_{ns}^k = \boldsymbol{0} \end{aligned} \tag{10}$$

with boundary conditions

$$\boldsymbol{u}_\tau^k = \overline{\boldsymbol{u}}_\tau^k \; or \; \boldsymbol{\Pi}_u^{k\tau s} \boldsymbol{u}_s^k + \boldsymbol{\Pi}_\sigma^{k\tau s} \boldsymbol{\sigma}_{ns}^k = \boldsymbol{\Pi}_u^{k\tau s} \overline{\boldsymbol{u}}_s^k + \boldsymbol{\Pi}_\sigma^{k\tau s} \overline{\boldsymbol{\sigma}}_{ns}^k \tag{11}$$

When LW descriptions are used, the equations controlling the behavior of the layers are first derived at the individual layer level. The equations for the entire multilayer structure are then obtained by assuring the stresses and displacements remain continuous between the layers.

Materials Research Proceedings 31 (2023) 596-613 https://doi.org/10.21741/9781644902592-62

Navier-type closed form solution:
The aforementioned boundary value problems, in the broadest range of configurations and constraints, could be solved approximately. When the material displays orthotropic behavior, Navier-type analytical solutions can be derived by taking the harmonic forms of the applied loads and the unknown variables into account:

$$\begin{aligned}\left(u_{x_\tau}^k, \sigma_{xz_\tau}^k, p_{x_\tau}^k\right) &= \sum_{m,n}\left(U_x^k, S_{xz_\tau}^k, P_{x_\tau}^k\right)\cos\frac{m\pi x}{a}\sin\frac{n\pi y}{b}\\ \left(u_{y_\tau}^k, \sigma_{yz_\tau}^k, p_{y_\tau}^k\right) &= \sum_{m,n}\left(U_y^k, S_{yz_\tau}^k, P_{y_\tau}^k\right)\sin\frac{m\pi x}{a}\cos\frac{n\pi y}{b}\\ \left(u_{z_\tau}^k, \sigma_{zz_\tau}^k, p_{z_\tau}^k\right) &= \sum_{m,n}\left(U_z^k, S_{zz_\tau}^k, P_{z_\tau}^k\right)\sin\frac{m\pi x}{a}\sin\frac{n\pi y}{b}\end{aligned} \tag{12}$$

while m and n are the correspondent wave numbers. The maximum amplitudes corresponding to the RHS of Eq. (12) are represented by capital letters. This method has been implemented for different theories and the outcomes will be covered in the following sections. Any type of imposed force can be adjusted to the Navier form unless a suitable Fourier expansion is implemented. The benchmarks discussed in the following sections are related to various transverse pressure distributions p_{zT}, and the suitable Fourier expansion for these cases should be written as:

$$(p_{zT}) = \sum_{m,n}^{R,Q}(p_{zT}^{mn})\sin\frac{m\pi x}{a}\sin\frac{n\pi y}{b} \tag{13}$$

Where R and Q are the maximum values of the considered m and n, while p_{zT}^{mn} are the Fourier series coefficients. See Figure 2

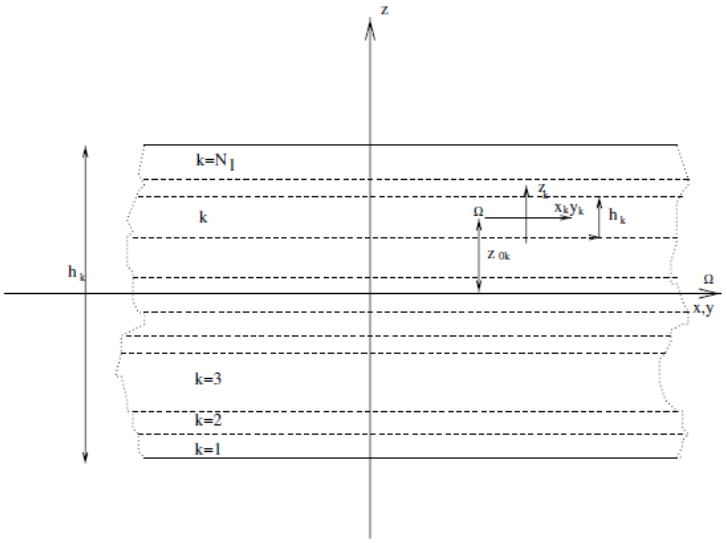

Figure 2 Plate geometry and notations

Numerical results and discussion
Three different geometrical test cases are introduced in this section: shell plate, shell cylindrical section and shell cylinder. For each test case different stacking sequence are analysed. Different thicknesses and lamination configurations will be considered for each test case.

Convergence Analysis
A preliminary study of convergence mesh is conducted for the commercial code to reduce the influence of the mesh on the results. The choice of element size made at this stage will also be adopted in the following cases. In Figure 1, the convergence analysis configuration is illustrated, where a render shell thickness is adopted to better appreciate the imposed boundary condition. The

plate is subjected to a uniform force acting along the z axes in opposite direction, a simply supported BC are applied on the four edge of the square plate and a ratio between the edge and the thickness equal 4 is considered.

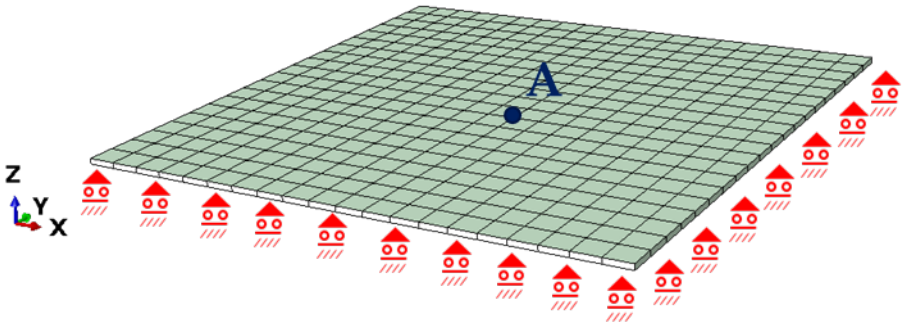

Figure 3 commercial software mesh convergence configuration

The results of the convergence analysis are shown in Table 1 where the first column reports the dimensions of the elements expressed as the ratio of the plate side size to the number of elements, the second column reports the displacement along the z-axis with respect to the maximum deflection. In accordance with Table 1, the choice of the dimension element equal to 20 was chosen to obtain a good mitigation of the effects due to the size of the elements and the computational cost.

Table 1 Mesh convergence analysis

Mesh Convergence

Dimension Element $\left[\frac{a}{n}\right]$	Max Deflection $\left[\frac{z}{z_{max}}\right]$
3	0.812
5	0.879
10	0.976
20	0.998
30	0.999
50	1

Simply supported cross-ply plate under pressure

The cross ply square base plate is subjected to a pressure with a bi-harmonic distribution expressed as a Fourier series with m and n equal to one (Figure 2). To assess the influence of thickness on the mechanical response of the structure, three different ratios of side length to thickness are considered $\left(\frac{a}{Th} = 4; 10; 20\right)$, where Th is the plate thickness.

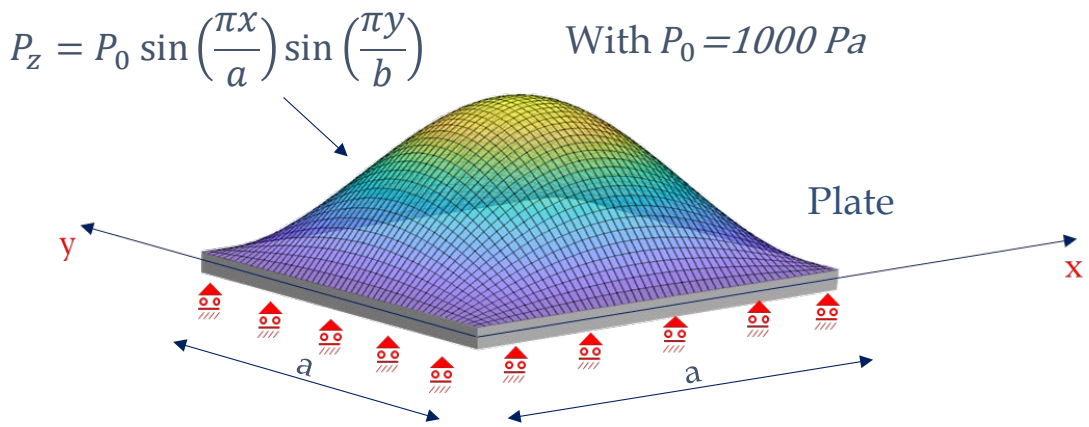

Figure 4 Square cross ply plate under biharmonic pressure load

The square cross-plate has simply supported condition on the four edges and a symmetrical stacking sequence of [0/90/0], where the mechanical properties adopted for the layered plate are expressed in accordance with Table 2.

Table 2 Mechanical Properties of the material

Material Properties		
Young's Modulus	E_L/E_T	30
Shear Modulus	G_{LT}/E_T	0.5
Shear Modulus	G_{TT}/E_T	0.35
Poisson	ν_{LT}	0.3
Poisson	ν_{TT}	0.49

The values of transverse displacement, tension in the L, T and LT directions of the central point of the plate were dimensionless in accordance with the equations 14a-d

$$\bar{U}_z = \frac{U_z 100 E_T h^3}{p_z a^4}; \quad \text{(a)} \qquad \bar{S}_{11} = \frac{S_{11}}{p_z (a/Th)^2}; \quad \text{(b)}$$

$$\bar{S}_{22} = \frac{S_{22}}{p_z (a/Th)^2}; \quad \text{(c)} \qquad \bar{S}_{12} = \frac{S_{12}}{p_z (a/Th)^2}; \quad \text{(d)} \tag{14}$$

Table 3 and Table 4 show the results obtained in accordance with Equations 14 a-d and pertain respectively the displacement values and the stress values. The values were obtained considering different theories. L refers to a Layer-Wise model, ED to an equivalent single layer model, FSDT to a first shear deformation theory model, CST to classic laminate theory. Furthermore, for the L and ED models, id 1 to 4 refer from linear to fourth order implemented expansions function in the plate/layer thickness z-direction [34]. The data on the maximum dimensionless plate displacement show that for thick structures values close to the 3D solution [37] are only equated by the Layer-wise model of order 4 and 3, while the other theories register an error ranging from 82% of the CST, to about 7.5 % of the commercial code through to about 27% of the FSDT. Moving from a thick to a very thin layered structure, the differences recorded between the various theories are greatly reduced, with a maximum variation of around 28% for the CST. The layer-wise approach

allows exact displacement values to be reproduced even with small expansion orders. The commercial code, in the case of thin plate, reduces its error to (in the configuration considered) 3.5%, representing a viable alternative to the CST, FSDT and ED theories with small expansion order values.

Table 3 Maximum value of displacement in z direction

	$\bar{U}_z$		
	4	***10***	***20***
3D	2.820	0.919	0.610
L4	2.821	0.919	0.609
L3	2.821	0.919	0.609
L2	2.798	0.918	0.609
L1	2.720	0.898	0.604
ED4	2.625	0.866	0.592
ED3	2.627	0.866	0.595
ED2	2.035	0.750	0.565
ED1	2.051	0.750	0.565
FSDT	2.051	0.750	0.563
CST	0.501	0.501	0.439
ABAQUS	2.611	0.865	0.589

The tension values in the longitudinal, transverse and shear directions are reported in Table 4. The values are referred to the midpoint of the plate, and the superscript '+' denotes the tension values evaluated on the top of the plate, while the superscript '-' denotes the values obtained on the bottom face of the laminate. Similar considerations to those made for displacement can be made in the evaluation of stresses. However, the greatest discrepancy in the evaluation of tension occurs in the longitudinal direction for the ED1 approach. Again, the values obtained with the commercial code, although close to the 3D solution [37], do not reach the degree of accuracy shown by the LW (1-4) and ED (2,3) approaches. Furthermore, the commercial code reports the same absolute tension value for the top and bottom of the laminate, while the other theories manage to record a variation in tension as shown by the benchmark.

Table 4 Stress distribution in longitudinal, transversal and shear distribution on the top and bottom of the plate

	$\bar{s}_{11}^{+}$	$\bar{s}_{12}^{+}$	$\bar{s}_{22}^{+}$	$\bar{s}_{11}^{-}$	$\bar{s}_{12}^{-}$	$\bar{s}_{22}^{-}$
	4	***10***	***20***	***4***	***10***	***20***
L4	15.52	1.374	0.4982	-15.02	1.385	0.4930
L3	15.53	1.373	0.4982	-15.02	1.293	0.4955
L2	15.33	1.357	0.4982	-14.99	1.293	0.4955
L1	14.27	1.367	0.4945	-13.86	1.290	0.4954
ED4	15.39	1.366	0.4977	-15.05	1.307	0.4953
ED3	15.51	1.360	0.4977	-14.22	1.325	0.4959
ED2	11.35	1.447	0.4977	-10.80	1.375	0.4956
ED1	10.98	1.443	0.4840	-12.25	1.385	0.5000
FSDT	11.17	1.443	0.5000	-12.22	1.402	0.5000
CST	13.48	1.691	0.500	-12.22	1.402	0.5000
ABAQUS	14.08	1.298	0.4936	-14.08	1.298	0.4936

Materials Research Proceedings 31 (2023) 596-613 https://doi.org/10.21741/9781644902592-62

Shell cylindrical section

The second benchmark analysed and reported on in this paper is the layered cylindrical section shown in Figure 5 A-B. The upper surface of the structure is subjected to a sinusoidal pressure distributed according to Figure 5-B, while simply supported conditions are applied along the extreme sides parallel to the generators. Both the pressure distribution and the boundary conditions are described considering a cylindrical reference system whose origin coincides with the central point of the upper surface, and whose three axes coincide with the direction of the generatrix (longitudinal direction), directrix (transverse direction) and normal to the surface, respectively (as shown in Figure 5-A), respectively.

To mitigate edge effects, a section length equal to four times the radius was considered.

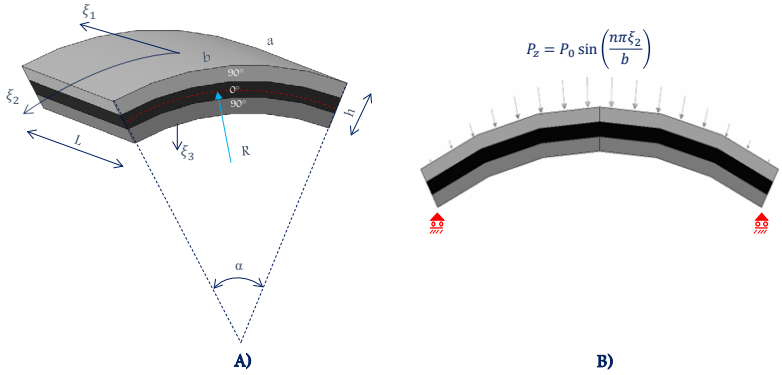

Figure 5 Cylinder shell section

The axisymmetric geometry shown in this section and studied in [33] is a cylindrical section consisting of three layers of orthotropic material with equal thickness. The cylindrical section was analysed considering four different thicknesses, where the configurations due to thickness variation will be identified through the parameter a, which expresses the ratio of the cylinder radius to the thickness of the laminate, the values being equal to $a = \frac{R}{Th} = 2; 4; 50; 500$.

According with [33] the stacking sequence for the cylinder section is equal to [0/90/0], while the mechanical properties of the material and some geometrical data are given in Table 5.

Table 5 Mechanical Properties

Material and Geometrical Properties		
Young's Modulus	E_L/E_T	25
Shear Modulus	G_{LT}/E_T	0.5
Shear Modulus	G_{TT}/E_T	0.2
Poisson's ratio	ν_{LT}/ν_{TT}	0.25
Radius	R	10
Angle span	α	$\pi/3$

The results shown in Table 4 refer to the radial displacement of the cylinder section evaluated at the origin of the cylindrical reference system. The results were obtained in accordance with Equation 14-a by evaluating the same theories discussed in the previous section. For very high thickness values, in contrast to the square plate, the variations with respect to the 3D solution are remarkably small. The ED1-4 solution underestimates the maximum value of the deflection just as it does for the CST theory, for some configurations of the LW theory and for the first shear order deformation theory. In contrast, approaching the problem with commercial software even in a small way returns a higher deflection value than the exact solution. The decrease in thickness

greatly mitigates the simplifications in dowry of the various theories used for this study. For very thin structures even the CST theory, which usually significantly underestimates the deflection values, provides results in line with the 3D solution.

Table 6 Maximum value of displacement in z direction. Section cylinder

	$\bar{U}_z$			
	2	4	50	500
3D	1.436	0.457	0.0808	0.773
L4	1.435	0.4581	0.08083	0.07767
L3	1.459	0.4614	0.08084	0.07767
L2	1.411	0.4576	0.08083	0.07767
L1	1.363	0.4407	0.08067	0.07764
ED4	1.383	0.4284	0.08051	0.07767
ED3	1.369	0.4272	0.08051	0.07767
ED2	1.111	0.3310	0.07982	0.07766
ED1	1.129	0.3324	0.07982	0.07766
FSDT	1.169	0.3329	0.07976	0.07766
CST	0.09625	0.08712	0.07834	0.07766
ABAQUS	1.4852	0.4561	0.08015	0.07739

Cylinder

The last test case discussed in this article consists of a cylinder made of composite material with a constant cross-section whose geometrical characteristics are shown in Figure 7 Each layer of the cylinder made of square symmetric unidirectional orthotropic fibrous material and the adopted properties are reported in Table 5. The results, applied load and boundary conditions were imposed in accordance with a cylindrical reference system whose axes coincide with the radial, tangential and axial direction of the cylinder (axial direction coincides with the longitudinal axis of the fibre for ply oriented at 0°)

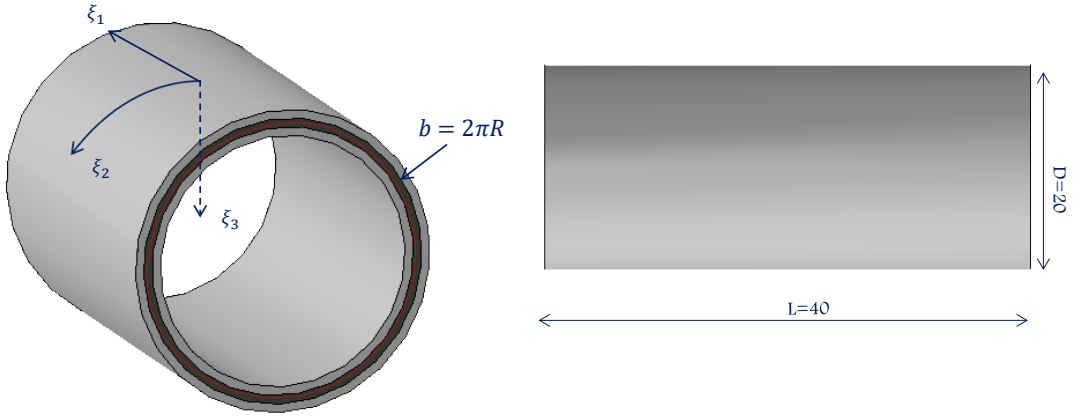

Figure 6 Geometrical description of cylinder case

The geometric variations in terms of thickness investigated are the same as reported in the previous section. In addition, two different stacking sequences are investigated, and for each of the two configurations 4 variations in thickness were analysed. For the [0/90] case, the first ply, oriented along the axis of the cylinder is positioned in the inner layer of the cylinder. A harmonic pressure is applied to the inner face of the cylinder, where the distribution is described by Equation 15, and the parameters m and n are respectively equal to1 and 8.

$$P_z = P_0 \sin\left(\frac{m\pi\xi_1}{L}\right) \sin\left(\frac{n\pi\xi_2}{b}\right) \quad (15)$$

The pressure distribution and boundary conditions are illustrated in Figure 8. In detail, the boundary conditions are of the simply supported type in accordance with the reference system previously illustrated and applied to the extreme edges of the cylinder.

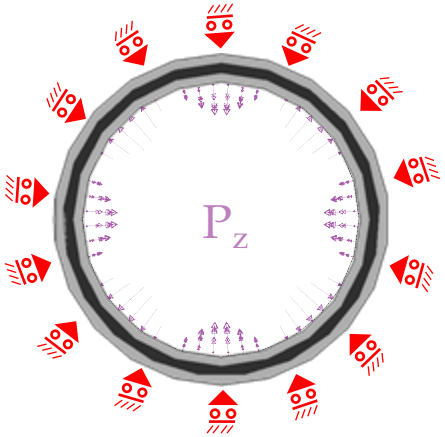

Figure 7 Applied boundary conditions.

Firstly, the results for the [90/0] stacking sequence are discussed and then the three plies configuration outcomes will be introduced. The values of maximum displacement are shown in Table 7, and evaluated following the equation 13-A, where the z direction is the radial direction of the cylinder or in a simpler way the ξ_3 of Figure 7. For the [0/90] plies configuration angle, Abaqus commits an error in the evaluation of the maximum displacement value, in the case of thick structures (a=2), of approximately 22.5% by overestimating the value obtained from the 3D solution. Of the used theories, the one underlying the commercial software is the only one that overestimates the value of the deflection so markedly. Except for the LD4 configuration, all other theories underestimate the exact value with more or less marked errors.

By reducing the thickness by a factor of two, the percentage errors committed by the various considered theories become significantly lower (except for CST). In addition, for a thickness value identified by a=4 configuration, the values given in the table are always lower than the exact value except for the L4 configuration, which tends to overestimate the exact solution, albeit with an error of about 1%.By increasing the term a (decreasing the value of the thickness), the structural response in terms of maximum deflection is at the exact value for all theories, with the exception of the value obtained with the Abaqus software, which again tends to overestimate the exact value and records the value that deviates the most from that reported in [33].

Table 7 Cylinder axial displacement

	$\bar{U}_z$			
	2	**4**	**50**	**500**
3D	14.034	6.100	2.242	0.1005
L4	14.33	6.164	2.242	0.1007
L2	13.80	5.921	2.241	0.1007
ED4	14.08	6.075	2.242	0.1007
ED2	13.07	5.717	2.240	0.1007
FSDT	12.41	5.578	2.240	0.1007
CST	2.781	2.802	2.227	0.1007
ABAQUS	17.197	5.944	2.234	0.1011

Materials Research Proceedings 31 (2023) 596-613 https://doi.org/10.21741/9781644902592-62

The values of the stresses in the L (Longitudinal) and LT directions are shown in Table 7. For each theory, the first line shows the stress value obtained on the external surface while the second line shows the stress values evaluated on the internal surface. Comparing the results obtained from the theories considered, for both directions 11 and 12, with the 3D reference values shows a marked underestimation for both classical theories and the Abaqus model for thick structures. The decrease in thickness induces a progressive reduction in the error. In fact, for very thin structures, the stress values tend to the correct value regardless of the theory considered. This case study, unlike the previous cases, shows a less pronounced variation of results in the case of thick structures.

Table 8 Stresses value for direction L and LT

	S_{11}				S_{12}			
	2	**4**	**50**	**500**	**2**	**4**	**50**	**500**
3D	-2.660	-0.9610	1.610	0.9436	-0.5016	-0.2812	-0.3449	-0.1045
	0.2511	0.2120	0.2189	0.0449	0.2685	0.2007	-0.0784	-0.0925
L4	-2.678	-0.9557	1.606	0.9484	-0.4910	-0.2859	-0.3606	-0.1099
	0.2578	0.2210	0.2241	0.04536	0.3067	0.2216	-0.08282	-0.09736
L2	-2.610	-0.9386	1.605	0.9484	-0.4631	-0.2732	-0.3603	-0.1099
	0.19686	0.1732	0.2204	0.04534	0.2861	0.2103	-0.08276	-0.09736
ED4	-2.649	-0.9580	1.605	0.9486	-0.4812	-0.2831	-0.3605	-0.1099
	0.2302	0.2181	0.2216	0.04516	0.3032	0.2199	-0.08280	-0.09736
ED2	-2.172	-0.8725	1.606	0.9483	-0.3677	-0.2521	-0.3602	-0.1099
	0.1049	0.1156	0.2226	0.04567	0.2541	0.2025	-0.08275	-0.09736
FSDT	-1.216	-0.6911	1.603	0.9484	-0.2994	-0.2431	-0.3604	-0.1099
	0.2256	0.2018	0.2236	0.04535	0.2532	0.1946	-0.08313	-0.09736
CST	-0.5690	-0.4752	1.594	0.9484	-0.1534	-0.1761	-0.3588	-0.1099
	0.1464	0.1661	0.2230	0.04535	0.1504	0.1516	-0.08235	-0.09736
ABAQUS	-1.6875	-0.79688	1.6076	0.9432	0.3153	0.2338	-0.3442	-0.1045
	0.3120	0.23544	0.20310	0.04508	0.2945	-0.2015	0.1567	-0.0926

Furthermore, with the classical CST theories, FSDT and commercial codes such as Abaqus, it is not possible to evaluate stresses in the 33 direction (radial direction) and 23 directions. Using high order theories allows both the layer-wise approach and the equivalent single layer approach to evaluate the stress distribution in the 23 and 33 directions, thus obtaining more accurate numerical models.

Table 9 Stresses value for 23 and 33 directions on cylinder case.

	S_{23}				S_{33}			
	2	***4***	***50***	***500***	***2***	***4***	***50***	***500***
3D	-2.931	-4.440	-4.785	-0.227	-0.31	-0.7	-6.29	-3.09
L4	-3.216	-4.791	-5.024	-0.2441	-0.3408	-0.7358	-6.549	-3.082
ED4	-2.928	-4.274	-3.395	0.2764	-0.3358	-0.7126	-5.072	4.793

For the cylinder case, as previously introduced at the beginning of this section, two different stacking sequences were considered. For the case [0/90], the results have already been discussed, while the results for the stacking configuration of [0/90/0] will now be introduced. Results from previous case studies show that the best results for high order theories are provided by the layer-

Materials Research Proceedings 31 (2023) 596-613 https://doi.org/10.21741/9781644902592-62

wise and equivalent single layer approach. Noting this aspect, to make the results clearer and to highlight the discrepancies in the values obtained from the exact solution [9] and finite element approach with the code introduced in [33] and Abaqus code, the comparisons was only made between 3D, L4, ED4 and Abaqus.

Table 10 Radial displacement for [0/90/0] cylinder configuration

	$\bar{U}_z$			
	2	**4**	**50**	**500**
3D	10.1	4.009	0.5495	0.1027
L4	10.1	4.032	0.5495	0.1027
ED4	9.1582	3.7197	0.5458	0.1027
ABAQUS	19.045	5.2111	0.5538	0.1031

Table 9 shows the values of the radial displacements calculated according to the kk formula. The results again show that for thick structures, the approach using commercial software, in this case, Abaqus, yields a value of approximately twice the reference value. Higher-order theories, albeit with different approaches, provide values very similar to the 3D solution. By moving from thicker to thinner structures, it is possible to obtain a maximum cylinder deflection that tends very closely to the 3D solution. Obviously, high order theories can perfectly reproduce the maximum radial displacement value for the cylinder.

Table 11 Stresses in direction 11 and 12 for [0/90/0] cylinder test case

	S_{11}				S_{12}			
	2	**4**	**50**	**500**	**2**	**4**	**50**	**500**
3D	-0.8428	-0.2701	-0.0225	0.0379	-0.2922	-0.1609	-0.0760	-0.0889
	0.1761	0.1270	0.0712	0.0559	0.1797	0.1081	-0.0181	-0.0766
L4	-0.8604	-0.2733	-0.0241	0.0377	-0.2918	-0.1642	-0.0795	-0.0935
	0.1841	0.1330	0.0734	0.0565	0.2015	0.1175	-0.0124	-0.0806
ED4	-0.9447	-0.3011	-0.0240	0.0381	-0.2770	-0.1568	-0.0791	-0.0935
	0.1433	0.1167	0.0730	0.0568	0.1957	0.1127	-0.0123	-0.0806
ABAQUS	-0.21450	-0.1117	-0.02136	0.03793	-0.2883	-0.1504	-0.0755	-0.0887
	0.14583	0.07656	0.07152	0.05604	0.2094	0.0968	-0.0352	-0.0769

Table 10 shows the values of the stresses evaluated in direction 11 and direction 12. Unlike the radial displacement trend, in the case of thick structures the use of high order theories with a layer-wise approach can provide values close to the reference solution. In fact, using an equivalent single-layer approach commits a percentage error of approximately 10%. Finally, using the commercial Abaqus code commits a percentage error of around 75%. The percentage errors evaluated above refer to the s11 tension case and evaluating the maximum error percentages, i.e. not taking into account whether the maximum tension error is evaluated on the outer or inner surface of the cylinder. Moreover, in Table 10, the values of the voltages in the direction 12 are given in the section of the table. A trend of the values of the voltages is noticed like that described by the direction 11 even if with different percentage variations.

Finally, the results of the stresses in Directions 23 and 33 are given in Table 12. It is important to note that in the table the corresponding values for the commercial software Abaqus are not reported, this is due to the impossibility of the commercial code to provide a stress state in all directions, with the use of shell elements (S4). Instead, high order theories allow us to obtain the

stresses in the considered directions and in the radial direction (thickness direction) comparable with the 3D reference values. In detail, once again the layer-wise approach makes it possible to correctly assess the stress state both for thick structures and for structures with low thickness. While the equivalent single layer approach provides approximate values like the reference values for thick structures, it tends to underestimate the value of tension in the case of thin structures.

Table 12 Stresses in direction 11 and 12 for [0/90/0] cylinder test case

	S_{23}				S_{33}			
	2	**4**	**50**	**500**	**2**	**4**	**50**	**500**
3D	-1.379	-2.349	-3.491	-0.691	-0.34	-0.62	-4.85	-9.12
L4	-1.442	-2.464	-3.659	-0.7287	-0.343	-0.627	-5.026	-9.468
ED4	-1.280	-2.025	-2.613	-0.5195	-0.358	-0.684	-5.184	-12.26

Conclusion

In this paper, different static shell and plate finite element analyses based on the CUF formulation were presented. The analysis involved three different benchmarks with three different geometries of different complexity. Different theories were compared to evaluate the performance of the shell elements considering the classical theories and the refined ones (high order) [33-36], in addition to the comparison was introduced a model made with the commercial software Abaqus. The results were provided for different thickness values (from extremely thick structures to extremely thin structures) in terms of displacement, tension in the plane and out of the plane where it could be evaluated. In accordance with what has been shown, shell elements based on the unified formulation of Carrera both with layer-wise approach and with equivalent single layer approach are not subject to shear locking phenomena, even for extremely thin structures. Also, for any thickness value. Obviously for excessively thick structures can be used a shell modelling provided that the expansion orders of the functions of the displacement in the direction of the thickness are increased. However, the use of classical theories such as CST and FSDT can only be used with very thin layered structures. On the other hand, commercial software can provide acceptable results for relatively thin structures while for thick structures, although it can provide results affected by a minor error compared to the solutions obtained by classical theories, are however not acceptable because suffering from an error too high. In addition, layer-wise models work better than equivalent single layer models, which in turn provide more accurate results when compared to business codes. To conclude the use of LW models is required for both thick and thin shells if the distribution of transverse tresses in the thickness is to be correctly described and the interlaminar continuity requirements are to be met. Neglecting that the high order models manage to provide a situation of tensions both in the plan and out of the plan unlike the commercial codes that neglect the trend of tensions outside the plan, providing therefore an approximate resolution of the analysed problem.

References

[1] Ambartsumyan VA. In: Ashton JE, editor. Theory of anisotropic plates. Tech Pub Co; 1969. Translated from Russian by T Cheron.

[2] Reddy JN. Mechanics of laminated composite plates, theory and analysis. CRC Press; 1997.

[3] Noor AK, Rarig PL. Three-dimensional solutions of laminated cylinders. Computer Methods in Applied Mechanics and Engineering 1974; 3:319-334. https://doi.org/10.1016/0045-7825(74)90017-6

[4] Malik M. Differential quadrature method in computational mechanics: new development and applications. Ph.D Dissertation, University of Oklahoma, Oklahoma, 1994.

[5] Liew KM, Han B, Xiao M. Differential quadrature method for thick symmetric cross-ply laminates with first-order shear flexibility. International Journal of Solids and Structures 1996; 33:2647-2658. https://doi.org/10.1016/0020-7683(95)00174-3

[6] Ferreira AJM, Roque CC, Carrera E, Cinefra M. Analysis of thick isotropic and cross-ply laminated plates by radial basis functions and unified formulation. Journal of Sound and Vibration 2011; 330:771-787. https://doi.org/10.1016/j.jsv.2010.08.037

[7] Ferreira AJM, Roque CC, Carrera E, Cinefra M, Polit O. Analysis of laminated shells by a sinusoidal shear deformation theory and radial basis functions collocation, accounting for through-the-thickness deformations. Composites Part B 2011; 42:1276-1284. https://doi.org/10.1016/j.compositesb.2011.01.031

[8] Reddy JN, Robbins DH. Theories and computational models for composite laminates. Applied Mechanics Review 1994; 47:147-165. https://doi.org/10.1115/1.3111076

[9] Varadan TK, Bhaskar K. Review of different theories for the analysis of composites. Journal of Aerospace Society of India 1997; 49:202-208.

[10] Carrera E. Developments, ideas and evaluations based upon Reissner's mixed variational theorem in the modeling of multilayered plates and shells. Applied Mechanics Review 2001; 54:301-329. https://doi.org/10.1115/1.1385512

[11] Argyris JH. Matrix displacement analysis of plates and shells, Prolegomena to a general theory, part I. Ingeniur-Archiv 1966; 35:102-142. https://doi.org/10.1007/BF00536183

[12] Sabir AB, Lock AC. The application of finite elements to the large deflection geometrically non-linear behaviour of cylindrical shells. In Variational Methods in Engineering 2, Southampton University Press: 1972; 7/66-7/75.

[13] Wempner GA, Oden JT, Kross DA. Finite element analysis of thin shells. Journal of Engineering Mechanics ASCE 94 1968; 94:1273-1294. https://doi.org/10.1061/JMCEA3.0001039

[14] Abel JF, Popov EP. Static and dynamic finite element analysis of sandwich structures. Proceedings of the Second Conference of Matrix Methods in Structural Mechanics, Vol. AFFSL-TR-68-150, Wright-Patterson Air Force Base, Ohio, USA, 1968; 213-245.

[15] Monforton GR, Schmidt LA. Finite element analyses of sandwich plates and cylindrical shells with laminated faces. Proceedings of the Second Conference of Matrix Methods in Structural Mechanics, Vol. AFFSL-TR-68-150, Wright-Patterson Air Force Base, Ohio, USA, 1968; 573-308.

[16] Noor AK. Finite element analysis of anisotropic plates. American Institute of Aeronautics and Astronautics Journal 1972; 11:289-307. https://doi.org/10.1002/nme.1620110206

[17] Hughes TJR, Tezduyar T. Finite elements based upon Mindlin plate theory with particular reference to the four-node isoparametric element. Journal of Applied Mechanics 1981; 48:587-596. https://doi.org/10.1115/1.3157679

[18] Parisch H. A critical survey of the 9-node degenerated shell element with special emphasis on thin shell application and reduced integration. Computer Methods in Applied Mechanics and Engineering 1979; 20:323-350. https://doi.org/10.1016/0045-7825(79)90007-0

[19] Zienkiewicz OC, Taylor RL, Too JM. Reduced intergration technique in general analysis of plates and shells. International Journal for Numerical Methods in Engineering 1973; 3:275-290. https://doi.org/10.1002/nme.1620030211

[20] Naghdi PM. The theory of shells and plates. In Handbuch der Physic, Vol. 4. Springer: Berlin, 1972; 425-640. https://doi.org/10.1007/978-3-642-69567-4_5

[21] Bathe KJ, Dvorkin EN. A four node plate bending element based on Mindlin/Reissner plate theory and mixed interpolation. International Journal for Numerical Methods in Engineering 1985; 21:367-383. https://doi.org/10.1002/nme.1620210213

[22] Arnold D.N., Brezzi F. Locking-free finite element methods for shells. Mathematics of Computation 1997; 66(217):1-14 https://doi.org/10.1090/S0025-5718-97-00785-0

[23] Bischoff M, Ramm E. On the physical significance of higher-order kinematic and static variables in a threedimensional shell formulation. International Journal of Solids and Structures 2000; 37:6933-6960. https://doi.org/10.1016/S0020-7683(99)00321-2

[24] Simo JC, Rafai S. A class of mixed assumed strain methods and the method of incompatible modes. International Journal for Numerical Methods in Engineering 1990; 29:1595-1638. https://doi.org/10.1002/nme.1620290802

[25] Kant T, Owen DRJ, Zienkiewicz OC. Refined higher order C0 plate bending element. Computer & Structures 1982; 15:177-183 https://doi.org/10.1016/0045-7949(82)90065-7

[26] Polit O, Touratier M. A new laminated triangular finite element assuring interface continuity for displacements and stresses. Composite Structures 1997; 38(1-4):37-44. https://doi.org/10.1016/S0263-8223(97)00039-1

[27] Tessler A. A higher-order plate theory with ideal finite element suitability. Computer Methods in Applied Mechanics and Engineerings 1991; 85:183-205. https://doi.org/10.1016/0045-7825(91)90132-P

[28] Reddy JN. Mechanics of Laminated Composite Plates and Shells, Theory and Analysis. CRC Press: New York, USA, 1997

[29] Rao KM, Meyer-Piening HR. Analysis of thick laminated anisotropic composites plates by the finite element method. Composite Structures 1990; 15:185-213. https://doi.org/10.1016/0263-8223(90)90031-9

[30] Noor AK, Burton WS. Assessment of computational models for multi-layered composite shells. Applied Mechanics Review 1990; 43:67-97. https://doi.org/10.1115/1.3119162

[31] Reddy JN. An evaluation of equivalent single layer and layer-wise theories of composite laminates. Composite Structures 1993; 25:21-35. https://doi.org/10.1016/0263-8223(93)90147-I

[32] Rammerstorfer FG, Dorninger K, Starlinger A. Composite and sandwich shells. In Nonlinear Analysis of Shells by Finite Elements, Rammerstorfer FG (ed.). Springer-Verlag: Vienna, 1992; 131-194. https://doi.org/10.1007/978-3-7091-2604-2_6

[33] Cinefra M., Carrera E. Shell finite elements with different through-the-thickness kinematics for the linear analysis of cylindrical multilayered structures. International journal for numerical methods in engineering. 93:(2013), pp. 160-182. https://doi.org/10.1002/nme.4377

[34] Carrera E., Ciuffreda A., A unified formulation to assess theories of multilayered plates for various bending problems. Composite Structures 69 (2005) 271-293 https://doi.org/10.1016/j.compstruct.2004.07.003

[35] Carrera E. Theories and finite elements for multilayered anisotropic composite plates and shells. Archives of Computational Methods in Engineering 2002; 9:87-140. https://doi.org/10.1007/BF02736649

[36] Carrera E. Theories and finite elements for multilayered plates and shells: a unified compact formulation with numerical assessment and benchmarking. Archives of Computational Methods in Engineering 2003; 10(3):215-296. https://doi.org/10.1007/BF02736224

[37] Carrera E. A class of two-dimensional theories for multi-layered plates analysis. Atti Accad Sci Tor, Mem Sci Fis 1995;19-20:49-87.

[38] Murakami H. Laminated composite plate theory with improved in-plane response. J Appl Mech 1986; 53:661-6. https://doi.org/10.1115/1.3171828

[39] Meyer-Piening HR. Experiences with 'Exact' linear sandwich beam and plate analyses regarding bending, instability and frequency investigations. In: Proceedings of the Fifth International Conference On Sandwich Constructions, Zurich, Switzerland, September 5-7, vol. I.; 2000. p. 37-48.

[40] Pagano NJ. Exact solutions for composite laminates in cylindrical bending. J Compos Mater 1969;3:398-411. https://doi.org/10.1177/002199836900300304